Two Non-Convex Optimization Approaches for Joint Transmit Waveform and Receive Filter Design

Mohammad Mahdi Omati[a], Seyed Mohammad Karbasi[a,*], Arash Amini[a]

[a]*Department of Electrical Engineering, Sharif University of Technology, Tehran, Iran*

Abstract

This study presents two innovative approaches for jointly optimizing the radar transmit waveform and receive filter to improve the signal-to-interference-plus-noise ratio (SINR) for extended targets under signal-dependent interference. We operate under the assumption of incomplete information about the target impulse response (TIR), which is confined within a predefined uncertainty set. To ensure robustness against this uncertainty, we frame the problem as a max-min (worst-case) optimization. Additionally, we impose a constant modulus constraint (because it has the lowest possible peak-to-average power ratio (PAPR)) on the transmit waveform to guarantee our system operates close to saturation. To solve this, both approaches use a sequential optimization procedure, alternating between the transmit waveform and receive filter subproblems. The first approach employs the ADMM, decomposing each subproblem into a semi-definite programming (SDP) problem and a least squares problem with a fixed rank constraint, solvable via SVD. The second approach tackles the problem over two Riemannian manifolds: the sphere manifold for the receive filter and the product of complex circles for the transmit signal. By applying manifold optimization, the constrained problem is transformed into an unconstrained one within a restricted search space. The max-min problem is reformulated as a minimization problem, yielding a closed-form expression involving log-sum-exp. This is solved using the Riemannian conjugate gradient descent (RCG) algorithm, which builds on Euclidean conjugate gradient descent and utilizes the manifold's properties, such as the Riemannian metric and retraction. Our numerical results demonstrate the robustness and effectiveness of these methods across various uncertainty sets and target types.

Keywords: ADMM, max-min optimization, Riemannian conjugate gradient descent (RCG) algorithm, SVD.

1. Introduction

One of the main challenges in designing radar, sonar, and communication systems is the joint optimization of the transmit waveform and receive filter. With advancements in radar resolution, targets frequently exhibit

*Corresponding author

extended range properties on radar screens. Consequently, waveform design tailored for extended targets has emerged as a relevant and widely studied topic in the literature [1–26].

The concept of an extended target in radar, first introduced in [21], has described situations where the target's size exceeds the radar's resolution, covering multiple range cells on the radar display. With the expansion of radar bandwidth and advancements in high-resolution range profiling techniques, extended targets have become increasingly common in radar detection scenarios. Unlike point-like targets, the echoes from extended targets are not simply scaled-down versions of the transmit waveform. Instead, they are the result of the convolution between the target impulse response (TIR) and the transmit waveform [12, 27–29]. The TIR, which is used to characterize the scattering properties of extended targets, depends on both the physical attributes of the target and the radar frequency [15, 25, 28, 30]. Traditional processing techniques optimized for point-like targets may not be ideal for extended targets. For example, while a matched filter maximizes the output signal-to-interference-plus-noise ratio (SINR) for point-like targets, it is not necessarily optimal for extended targets. Consequently, optimizing radar transmitters and receivers for extended targets has been a major focus of research over the past decades [12, 13, 16, 25, 31]. Significant advancements in enhancing radar performance can be achieved through a detailed understanding of TIR or its descriptive model [30]. A variety of TIR models have been employed to optimize radar performance based on diverse criteria [32]. The journey to optimize radar waveforms for extended targets was initiated with [12], which investigated waveforms for both optimal detection and information extraction. In the pursuit of an optimal detection waveform, the author of [12] strived to maximize the output SINR with a deterministic TIR. Conversely, for information extraction waveforms, the TIR was represented by a random vector, and the transmit waveform design aimed at maximizing the mutual information (MI) between TIR and the received signal. Moreover, the minimum mean square error (MMSE) metric was utilized for TIR parameter estimation or range profiling, as discussed in [13, 31, 33]. According to [13], minimizing MMSE and maximizing MI result in identical optimal waveforms in an additive white Gaussian channel. For extended targets, these waveform design methods, along with works such as [6, 23, 24, 34], are based on having knowledge of the TIR. However, in practical applications, accurately determining the TIR is challenging due to its sensitivity to factors such as the target aspect angle (TAA) relative to the radar line-of-sight (LOS).

To address this problem, one strategy is to make an assumption that the TIR or power spectral density (PSD) is partially known through cognitive methods [35–37]. This approach has allowed the design of robust waveforms or filters [14, 17, 18, 22, 38], which have led to minimax optimization problems [39–41]. To handle the uncertainty of PSD, a minimax waveform design model for MIMO radar based on MI and MMSE criteria was introduced

in [14]. In [18, 22], waveforms were designed by maximizing the worst-case SINR under an energy constraint (EC), where the minimax optimization was solved by changing the order of maximization and minimization. However, the waveform designed under the EC does not meet the requirements of the radar transmitter due to its high peak-to-average ratio (PAR) [42, 43]. In the study [25], the constant modulus constraint was considered because radar amplifiers typically operate in a saturation condition, which prevents amplitude modulation in radar waveforms. Karbasi et al. [25] approximated the spherical TIR set by sampling from its boundary. This was followed by the optimization of the waveform and filter, carried out using a step-by-step procedure rooted in semidefinite relaxation (SDR) techniques [44]. Finally, they employed randomization methods, as referenced in [44, 45], to synthesize the transmit code and the receive filter. However, one limitation of this approach has been its sensitivity to the sample size. When fewer samples are used, the method has demonstrated significantly lower SINR performance and reliability compared to direct optimization without relaxation techniques. Moreover, solving the relaxed optimization problem initially and then applying randomization can yield a suboptimal solution.

1.1. Contributions

This paper presents two innovative approaches for jointly designing the transmit waveform and receive filter to improve SINR for extended targets in the presence of signal-dependent interference, while also adhering to an energy constraint. We assume partial knowledge of the TIR, which is constrained within a predefined uncertainty set. This set is obtained by sampling the actual TIR at various TAAs, derived from previous observations and tracking files, and is defined by their corresponding TIRs. Additionally, we impose a constant modulus constraint on the transmit waveform to ensure our system operates near saturation. To ensure robustness against this uncertainty, we frame the problem as a max-min (worst-case) optimization optimization. Both proposed methods utilize a sequential optimization process that alternates between the transmit waveform and the receive filter during the optimization procedure. The first approach decomposes each design problem into a semi-definite programming (SDP) problem and a least square function with a fixed rank constraint, using the alternating direction method of multipliers (ADMM) [46]. Actually, using ADMM to decompose the problem allows us to efficiently address the fixed rank constraint using singular value decomposition (SVD). We call this approach the alternating direction method of multipliers with semidefinite programming and singular value decomposition (ASSD). The second approach addresses the max-min problem by optimizing over two Riemannian manifolds: the sphere manifold for the receive filter and the product of complex circles for the transmit signal. Manifold optimization treats the constrained problem as an unconstrained one over a restricted search space. Here, we

transform our max-min problem into a minimization problem by approximating the maximum of the objective function using the log-sum-exp form. We then tackle the reformulated problem by utilizing specific properties of the manifold, such as the Riemannian metric and retraction, to develop a Riemannian gradient descent algorithm derived from the Euclidean conjugate gradient descent method. We name this approach log-sum-exp Riemannian conjugate gradient descent (LSE-RCG).

Our numerical results validate the robustness and efficiency of the proposed methods across various uncertainty sets and target types. A significant advantage of our methods is that they not only enhance the SINR but also do so for the worst-case scenario. In other words, our strategies improve the SINR for every element of the uncertainty set, outperforming the methods proposed in previous studies. Additionally, our methods achieve convergence with fewer iterations compared to the main competitor [25], and even one of our approaches is faster in runtime too, indicating a reduction in computational resources. This advancement highlights the effectiveness of our strategies in enhancing radar system performance. The remainder of the paper is organized as follows. In Section 2, we begin by introducing the system model, detailing the target response, and examining the statistical properties of interference noise. Section 3 then outlines the optimization problem within a specific uncertainty set of TAAs. Following this, Section 4 presents our detailed strategies for the joint design of the waveform-filter pair and discusses the computational complexity involved in our proposed methods. In Section 5, we analyze simulation results, first considering three distinct uncertainty sets and then examining two different types of targets. Finally, Section 6 summarizes our findings and draws conclusions based on the research presented.

Notations. In this paper, we represent vectors and matrices using boldface letters: vectors are indicated by lowercase boldface $\mathbf{a}$ and matrices by uppercase boldface $\mathbf{A}$. The transpose is denoted by $(.)^T$, while the conjugate transpose is indicated by $(.)^H$. The identity matrix is represented as $\mathbf{I}$, and $\mathbf{0}$ signifies a matrix or vector with all zero elements, with sizes understood from the context. The set of N-dimensional complex vectors is denoted by $\mathbb{C}^N$, and $\mathbb{H}^N$ denotes the set of $N \times N$ Hermitian matrices. The Euclidean norm of a vector $\mathbf{a}$ is written as $\|\mathbf{a}\|_2$. The notation $|\mathbf{a}|$ refers to a vector whose elements are the absolute values of the elements of $\mathbf{a}$. The Hadamard product is denoted by $\odot$, and the convolution operator by $*$. We represent the objective function of the optimization problem $\mathcal{P}$ as $\text{obj}(\mathcal{P})$ and denote the optimal value as $v(\mathcal{P})$. The expectation operator is indicated by $\mathbb{E}[\cdot]$. Finally, $\mathcal{N}(\mathbf{0}, \mathbf{\Sigma})$ represents a zero-mean complex Gaussian distribution with a covariance matrix $\mathbf{\Sigma}$.

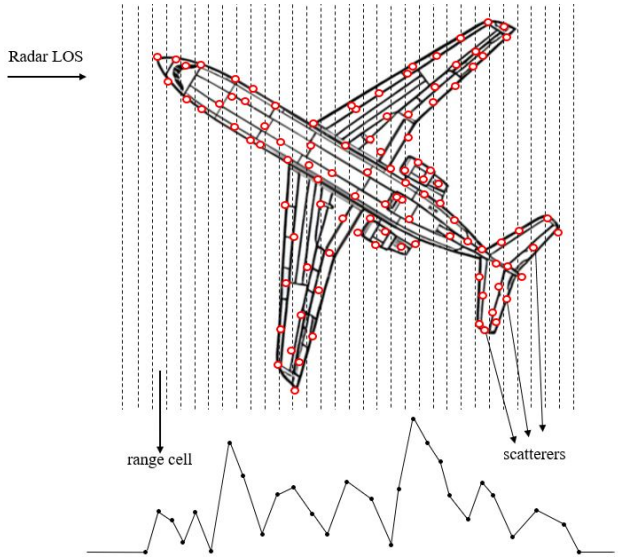

Figure 1: Return wave from scattering centers located in the range of radar visibility.

2. Target and Signal Model

2.1. Target Model

In high-resolution radar systems, the size of the range cell is considerably smaller than the physical dimensions of extended targets. This makes it insufficient to model the target as a single-point scatterer. Instead, the target is represented by its dominant scattering centers, which ensures that significant returns are confined to specific range cells along the radar's LOS. To accurately model this, the target is treated as a linear system with a finite impulse response (FIR). The parameters of this system are based on the target's shape and LOS [47–49]. It is widely recognized for its pronounced sensitivity to minor alterations in the orientation of the target. Fig. 1 illustrates the formation of TIR by projecting the scattering centers onto the LOS.

2.2. Signal Model

In our analysis, we concentrate on a monostatic radar setup, where the transmitted signal is described by an N-dimensional fast-time code:

$$\mathbf{s} = [s(0), ..., s(N-1)]^T \in \mathbb{C}^N. \tag{1}$$

When the target is surrounded by clutter, the discrete-time baseband equivalent of the return signal from

the extended target can be described as follows:

$$r(n) = \sum_{k=0}^{N-1} [h_\theta(n-k) + c(n-k)]s(k) + \upsilon\,(n) = [h_\theta(n) + c(n)] * s(k) + \upsilon\,(n). \tag{2}$$

In (2), the variable n indicates the discrete time index, and $h_\theta(n)$ represents the TIR corresponding to the TAA θ. The TIR $h_\theta(n)$ is assumed to be nonzero only within a support interval of length Q, meaning $h_\theta(n) = 0$ for n outside the range $\{0, \ldots, Q-1\}$. The term $c(n)$ represents the clutter impulse response (CIR), and $v(n)$ denotes receiver noise. The TIR vector is defined as $\mathbf{h}_\theta = [h_\theta(0), \ldots, h_\theta(Q-1)]^T \in \mathbb{C}^Q$. All observations $r(n)$ of the desired target are collected into a vector $\mathbf{r} = [r(0), \ldots, r(M-1)]^T \in \mathbb{C}^M$, where $M = Q + N - 1$ represents the total number of discrete time observations. This observation vector is expressed as:

$$\mathbf{r} = \mathbf{T}_\theta \mathbf{s} + \mathbf{C}\mathbf{s} + \boldsymbol{\upsilon}, \tag{3}$$

where $\boldsymbol{\upsilon} = [\upsilon(0), \ldots, \upsilon(M-1)]^T$ represents the additive noise component. $\mathbf{C} = \sum_{n=-N+1}^{M-1} c(n)\mathbf{J}_n$ and $\mathbf{T}_\theta = \sum_{n=0}^{q-1} h_\theta(n)\mathbf{J}_n$ are, respectively, the CIR and the TIR matrices, where $\mathbf{J}_n$ is the $M \times N$-dimensional shift matrix:

$$\mathbf{J}_n(\alpha_1, \alpha_2) = \begin{cases} 1, & if \quad \alpha_1 - \alpha_2 = n \\ 0, & if \quad \alpha_1 - \alpha_2 \neq n \end{cases}, \tag{4}$$

$$\alpha_1 = \{1, 2, .., M\}, \alpha_2 = \{1, 2, .., N\}. \tag{5}$$

Assuming the noise vector $\boldsymbol{\upsilon}$ to be circularly symmetric, we characterize it by the following statistical properties:

$$\mathbb{E}[\boldsymbol{\upsilon}] = 0, \tag{6}$$

$$\boldsymbol{\Sigma}_{\boldsymbol{\upsilon}} = \mathbb{E}[\boldsymbol{\upsilon}\boldsymbol{\upsilon}^H] = \sigma_{\boldsymbol{\upsilon}}^2 \mathbf{I}. \tag{7}$$

Here, $\sigma_{\boldsymbol{\upsilon}}^2$ represents the variance of each filtered noise sample. In addition, we make the assumption that the clutter has a zero mean, represented as $\mathbb{E}[c(n)] = 0$, and it is independent from the noise random process. Due to the high sensitivity of TIR to changes in TAA, giving an exact specification of TIR might not accurately represent the real world. Thus, the true TIR is considered to fall within a finite uncertainty set $\mathcal{I}$, which is

generated by sampling the TIR across various TAAs. We define the uncertainty set $\mathcal{I}_{\phi_1}^{\phi_2}$ of length K as follows:

$$\mathcal{I}_{\phi_1}^{\phi_2} = \{k\Delta\theta \mid k \in \mathbb{Z}, k\Delta\theta \in [\phi_1, \phi_2]\}, \tag{8}$$

where $\Delta\theta$ represents the TAA sampling step, and ϕ_1 and ϕ_2 define the lower and upper bounds of the TAA set, respectively. Our goal is to optimize the waveform-filter pair to maximize the worst-case SINR across the uncertainty set of TIRs. More details on the formulation of this worst-case optimization problem will be discussed in the following section.

3. Problem Formulation

In this section, our attention is directed towards formulating the problem for designing the waveform-filter pair. Assuming that the observation vector $\mathbf{r}$ is filtered through $\mathbf{w} = [w(0), ..., w(M-1)]^T \in \mathbb{C}^M$, the SINR at the filter output can be expressed as:

$$\mathrm{SINR}_\theta(\mathbf{s}, \mathbf{w}) = \frac{\left|\mathbf{w}^H \mathbf{T}_\theta \mathbf{s}\right|^2}{\mathbb{E}\left[\left|\mathbf{w}^H \mathbf{C}\mathbf{s}\right|^2\right] + \mathbb{E}\left[\left|\mathbf{w}^H \boldsymbol{\upsilon}\right|^2\right]}. \tag{9}$$

To ensure our system can operate near saturation, we impose a constant modulus constraint on the transmit waveform, which can be equivalently considered as applying a unit energy constraint on the transmit waveform, i.e., $\|\mathbf{s}\|_2^2 = 1$, along with the lowest possible upper bound for the PAR constraint:

$$\mathrm{PAR} = \frac{\max\limits_{n=0,\dots,N-1} |s(n)|^2}{\frac{1}{N}\|\mathbf{s}\|_2^2} = \max_{n=0,\dots,N-1} N|s(n)|^2 \leq 1. \tag{10}$$

As a result, our optimization problem can be formulated as:

$$\begin{aligned} \mathcal{P}: \quad & \max_{\mathbf{s},\mathbf{w}} \min_{\theta} \quad \mathrm{SINR}_\theta(\mathbf{s}, \mathbf{w}) \\ & \text{s.t.} \quad \|\mathbf{s}\|_2^2 = 1 \\ & \qquad |s(n)|^2 \leq \frac{1}{N}, \quad n = 0, ..., N-1. \end{aligned} \tag{11}$$

In order to simplify our SINR optimization process, we introduce the rank-one code and filter matrices as $\mathbf{S} = \mathbf{s}\mathbf{s}^H$ and $\mathbf{W} = \mathbf{w}\mathbf{w}^H$, respectively. Utilizing these definitions, we derive two equivalent expressions for

equation (9):

$$\mathrm{SINR}_\theta(\mathbf{s},\mathbf{w}) = \frac{\mathbf{w}^H \boldsymbol{\Gamma}(\mathbf{T}_\theta,\mathbf{S})\mathbf{w}}{\mathbf{w}^H \boldsymbol{\Sigma}_{\mathbf{C}\boldsymbol{\upsilon}}(\mathbf{S})\mathbf{w}} = \frac{\mathbf{s}^H \bar{\boldsymbol{\Gamma}}(\mathbf{T}_\theta,\mathbf{W})\mathbf{s}}{\mathbf{s}^H \bar{\boldsymbol{\Sigma}}_{\mathbf{C}\boldsymbol{\upsilon}}(\mathbf{W})\mathbf{s}}, \tag{12}$$

where

$$\boldsymbol{\Gamma}(\mathbf{T}_\theta,\mathbf{S}) = \mathbf{T}_\theta \mathbf{S} \mathbf{T}_\theta^H, \tag{13}$$

$$\boldsymbol{\Sigma}_{\mathbf{C}\boldsymbol{\upsilon}}(\mathbf{S}) = \mathbb{E}\left[\mathbf{C}\mathbf{S}\mathbf{C}^H\right] + \sigma_{\boldsymbol{\upsilon}}^2 \mathbf{I}, \tag{14}$$

$$\bar{\boldsymbol{\Gamma}}(\mathbf{T}_\theta,\mathbf{W}) = \mathbf{T}_\theta^H \mathbf{W} \mathbf{T}_\theta, \tag{15}$$

$$\bar{\boldsymbol{\Sigma}}_{\mathbf{C}\boldsymbol{\upsilon}}(\mathbf{W}) = \mathbb{E}[\mathbf{C}^H \mathbf{W} \mathbf{C}] + \sigma_{\boldsymbol{\upsilon}}^2 \mathrm{tr}(\mathbf{W})\mathbf{I}. \tag{16}$$

For a thorough explanation of the derivation of the SINR formulation (12), please refer to the Appendix A. In the subsequent section, we delve into our proposed methodologies regarding the optimization of $\mathbf{s}$ and $\mathbf{w}$ within the context of the worst-case problem $\mathcal{P}$.

4. Design of the waveform-filter pair

In this section, we are set to explore the jointly design of the transmit waveform and the receive filter. This is achieved by a process of alternating optimization between the receive filter and the transmit waveform. Initially, we concentrate on optimizing the receive filter, under the assumption that $\mathbf{s}$ remains fixed. Following this, we shift our focus towards optimizing the transmit signal, under the assumption that the receive filter $\mathbf{w}$ remains fixed. We persist in alternating between these two procedures until we arrive at the optimal solutions for both $\mathbf{w}$ and $\mathbf{s}$.

In examining the optimization problem $\mathcal{P}$, we see that scaling $\mathbf{w}$ by a constant does not impact the objective function since it affects both the numerator and denominator equally. Thus, we can add the constraint $\|\mathbf{w}\|_2^2 = 1$ to the problem. As a result, when we solve the optimization problem alternately, we get:

$$\begin{aligned} \mathcal{P}_{\mathbf{w}}^{(m)}: \quad & \max_{\mathbf{w}} \min_{\theta \in \mathcal{I}_{\phi_1}^{\phi_2}} \quad \frac{\mathbf{w}^H \boldsymbol{\Gamma}(\mathbf{T}_\theta,\mathbf{S}^{(m-1)})\mathbf{w}}{\mathbf{w}^H \boldsymbol{\Sigma}_{\mathbf{C}\boldsymbol{\upsilon}}(\mathbf{S}^{(m-1)})\mathbf{w}} \\ & \text{s.t.} \qquad \|\mathbf{w}\|_2^2 = 1, \end{aligned} \tag{17}$$

$$\mathcal{P}_{\mathbf{s}}^{(m)}: \quad \begin{aligned} \max_{\mathbf{s}} \min_{\theta \in \mathcal{I}_{\phi_1}^{\phi_2}} \quad & \frac{\mathbf{s}^H \bar{\mathbf{\Gamma}}(\mathbf{T}_\theta, \mathbf{W}^{(m)})\mathbf{s}}{\mathbf{s}^H \bar{\mathbf{\Sigma}}_{\mathbf{C}\boldsymbol{\upsilon}}(\mathbf{W}^{(m)})\mathbf{s}} \\ \text{s.t.} \quad & \|\mathbf{s}\|_2^2 = 1 \\ & |s(n)| \leq \frac{1}{\sqrt{N}}, \quad n = 0, ..., N-1. \end{aligned} \tag{18}$$

If we define

$$\text{SINR}^{(m)} = \text{SINR}\left(\mathbf{S}^{(m)}, \mathbf{W}^{(m)}\right), \tag{19}$$

where $\left\{\left(\mathbf{S}^{(m)}, \mathbf{W}^{(m)}\right)\right\}$ denotes a sequence of points produced by the proposed sequential optimization method, we set the stopping criterion as:

$$|\,\text{SINR}^{(m)} - \text{SINR}^{(m-1)}\,| \leq \eta. \tag{20}$$

The proposed sequential process demonstrates several interesting properties, as described in the following proposition.

Proposition 1. *Suppose that $\mathcal{P}_{\mathbf{w}}^{(m)}$ and $\mathcal{P}_{\mathbf{s}}^{(m)}$ are solvable, meaning each is feasible, bounded, and has an attainable optimal value. Then, it can be proven that the sequence $\left\{\text{SINR}^{(m)}\right\}$ is monotonically increasing and converges to a finite value. For the proof, refer to Appendix B.*

In the forthcoming discussion, we will address the optimization problem of designing the transmit waveform $\mathbf{s}$ and the receive filter $\mathbf{w}$ using two distinct approaches. Recognizing the similarity in optimizing $\mathbf{s}$ and $\mathbf{w}$, to avoid repetition of their structure, we intend to present each of our proposed approaches in a unified manner.

4.1. ASSD Approach

Let us consider the optimization problem $\bar{\mathcal{P}}_1$, where $\mathbf{x}$ represents the continuous variable and k indicates the discrete variable, which corresponds to the k^{th} element of the uncertainty set $\mathcal{I}_{\phi_1}^{\phi_2}$ as defined in Section 2:

$$\bar{\mathcal{P}}_1: \quad \begin{aligned} \max_{\mathbf{x}} \min_{k \in 1,2,...,K} \quad & \frac{\mathbf{x}^H \mathbf{A}_k \mathbf{x}}{\mathbf{x}^H \mathbf{B} \mathbf{x}} \\ \text{s.t.} \quad & \|\mathbf{x}\|_2^2 = 1 \\ & |x(n)|^2 \leq \gamma, \quad n = 0, ..., N-1. \end{aligned}$$

By setting $\gamma = 1$ and $\gamma = \frac{1}{N}$, the optimization problem $\bar{\mathcal{P}}_1$ transforms into $\mathcal{P}_{\mathbf{w}}$ and $\mathcal{P}_{\mathbf{s}}$ respectively. To streamline our objective function from a fractional quadratic form to a quadratic form, we seek to simplify it using the Dinkelbach approach [50–53], which we present as Lemma 1.

Lemma 1. *If we define our fractional function as follows:*

$$\mathcal{P}_{frac} : \max_{x} \left\{ Q(x) = \frac{N(x)}{D(x)} \mid x \in S \right\},$$

where $S \subseteq \mathbb{R}^2$ is nonempty and compact, and N and D are continuous functions on S with D being positive, the problem $\mathcal{P}_{frac}$ can be restated as:

$$\mathcal{P}_q : \max_{x} \{ N(x) - qD(x) \mid x \in S \}.$$

An optimal point x^+ for $\mathcal{P}_{frac}$ is optimal for $\mathcal{P}_{q^+}$, where q^+ is the unique root of:

$$F(q) = \max \{ N(x) - qD(x) \mid x \in S \},$$

with $q \in \mathbb{R}$. It is important to note that $q^+ = Q(x^+)$. Additionally, the function $F(q)$ is continuous, convex, and strictly decreasing on $\mathbb{R}$, with $F(q) > 0$ for $q < q^+$ and $F(q) < 0$ for $q > q^+$.

As per Lemma 1, we can reformulate $\bar{\mathcal{P}}_1$ as follows:

$$\bar{\mathcal{P}}_1^q : \begin{array}{lll} \max\limits_{\mathbf{x}} \min\limits_{k \in 1,2,\ldots,K} & \mathbf{x}^H \mathbf{C}_k \mathbf{x} \\ \text{s.t.} & \|\mathbf{x}\|_2^2 = 1. \\ & |x(n)|^2 \leq \gamma, \quad n = 0, ..., N-1. \end{array}$$

where $\mathbf{C}_k = \mathbf{A}_k - q\mathbf{B}$. Here, based on the Dinkelbach method, we start by fixing the parameter q and solving the problem $\bar{\mathcal{P}}_1^q$ for $\mathbf{x}$. Once we find the optimal $\mathbf{x}$, we update q by locating the root of $\text{obj}(\bar{\mathcal{P}}_1^q)$ with respect to q. This iterative procedure repeats until, at iteration l, the difference $\left| q^{(l)} - q^{(l-1)} \right|$ is less than a predefined tolerance η_D. For ease of reference, the iteration index l is dropped in the subsequent optimization problems.

By introducing the matrix $\mathbf{X}$ as $\mathbf{X} = \mathbf{x}\mathbf{x}^H$, we can reformulate $\bar{\mathcal{P}}_1^q$ as bellow:

$$\bar{\mathcal{P}}_2^q : \begin{array}{lll} \max\limits_{\mathbf{X}} \min\limits_{k \in 1,2,\ldots,K} & \text{tr}(\mathbf{C}_k \mathbf{X}) \\ \text{s.t.} & \text{tr}(\mathbf{X}) = 1 \\ & \mathbf{X} = \mathbf{X}^H \\ & \mathbf{X} \succeq \mathbf{0} \\ & \text{rank}(\mathbf{X}) = 1 \\ & \text{tr}(\mathbf{E}_n \mathbf{X}) \leq \gamma. \end{array}$$

It is important to highlight that, in the $\bar{\mathcal{P}}_2^q$ problem, we have utilized the definition of $\mathbf{E}_n$ as a matrix where only the $(n,n)^{\text{th}}$ entry is one and all other entries are zero to represent the constraint $|x(n)|^2 \leq \gamma, \quad n = 0, \ldots, N-1$,

in a matrix format. The transformation of problem $\bar{\mathcal{P}}_2^q$ into an equivalent one, which optimizes over the epigraph of the objective function, yields:

$$\bar{\mathcal{P}}_3^q: \begin{aligned} \max_{\mathbf{X},\alpha} \quad & \alpha \\ \text{s.t.} \quad & \operatorname{tr}(\mathbf{C}_k\mathbf{X}) \geq \alpha, \quad k \in 1,2,...,K \\ & \operatorname{tr}(\mathbf{X}) = 1 \\ & \mathbf{X} = \mathbf{X}^H \\ & \mathbf{X} \succeq \mathbf{0} \\ & \operatorname{rank}(\mathbf{X}) = 1 \\ & \operatorname{tr}(\mathbf{E}_n\mathbf{X}) \leq \gamma. \end{aligned}$$

To tackle $\bar{\mathcal{P}}_3^q$, we introduce the change of variables $\mathbf{X} = \mathbf{Z}$, enabling us to employ ADMM. Recently, numerous studies have focused on the convergence of ADMM for non-convex and non-smooth functions [54–59]. Drawing on the convergence proof provided in [58, 59]—due to the equivalence of our rank constraint with $\operatorname{rank}(\mathbf{X}) \leq 1$—we conclude that the optimization problem $\mathcal{P}_2^q$ satisfies the necessary conditions for applying ADMM. As a result, ADMM facilitates the isolation of the non-convex constraint $\operatorname{rank}(\mathbf{X}) = 1$ from the remaining constraints, and we derive:

$$\bar{\mathcal{P}}_4^q: \begin{aligned} \max_{\mathbf{X},\alpha,\mathbf{Z}} \quad & \alpha \\ \text{s.t.} \quad & \operatorname{tr}(\mathbf{C}_k\mathbf{X}) \geq \alpha, \quad k \in 1,2,...,K \\ & \operatorname{tr}(\mathbf{X}) = 1 \\ & \mathbf{X} = \mathbf{X}^H \\ & \mathbf{X} \succeq \mathbf{0} \\ & \operatorname{tr}(\mathbf{E}_n\mathbf{X}) \leq \gamma \\ & \mathbf{X} = \mathbf{Z} \\ & \operatorname{rank}(\mathbf{Z}) = 1. \end{aligned}$$

Hence, the related augmented Lagrangian (AL) function takes the form:

$$\mathcal{L}_\rho(\mathbf{X}, \alpha, \mathbf{Z}, \mathbf{R}) = \alpha - \langle \mathbf{R}, \mathbf{X} - \mathbf{Z} \rangle - \frac{\rho}{2} \|\mathbf{X} - \mathbf{Z}\|_F^2, \tag{21}$$

without directly associating other constraints with it. In (21), ρ is the penalty parameter, and $\mathbf{R}$ is the dual variable. Following this, we delve into the step-by-step procedure for updating $\mathbf{X}$, α, $\mathbf{Z}$, $\mathbf{R}$. It is crucial to note that during the update process for $\mathbf{X}$, $\mathbf{Z}$, and α, $\mathbf{R}$ is treated as a constant. As a result, the associated term can be conveniently expressed in Frobenius form, which is the intended representation.

4.1.1. Updating $\mathbf{X}$, α

When updating $\mathbf{X}$ and α, while keeping the variables $\mathbf{Z}$ and $\mathbf{R}$ unchanged, we have:

$$\bar{\mathcal{P}}_4^{\mathbf{X},\alpha}: \begin{aligned} \max_{\mathbf{X},\alpha} \quad & \alpha - \frac{\rho}{2}\left\|\mathbf{X}-\mathbf{Z}+\frac{\mathbf{R}}{\rho}\right\|_F^2 \\ \text{s.t.} \quad & \operatorname{tr}(\mathbf{C}_k\mathbf{X}) \geq \alpha, \quad k \in 1,2,...,K \\ & \operatorname{tr}(\mathbf{X}) = 1 \\ & \mathbf{X} = \mathbf{X}^H \\ & \mathbf{X} \succeq \mathbf{0} \\ & \operatorname{tr}(\mathbf{E}_n\mathbf{X}) \leq \gamma \end{aligned}$$

The SDP problem $\bar{\mathcal{P}}_4^{\mathbf{X},\alpha}$ is evidently convex and can be efficiently addressed using the CVX framework [60] in MATLAB and CVXPY [61, 62] in Python. In our work, we employed the CVX framework in MATLAB and used the SeDuMi solver to tackle this problem.

4.1.2. Updating $\mathbf{Z}$

Concerning the update of $\mathbf{Z}$, we arrive at the following optimization problem:

$$\bar{\mathcal{P}}_4^{\mathbf{Z}}: \begin{aligned} \min_{\mathbf{Z}} \quad & f(\mathbf{Z}) = \left\|\mathbf{X}-\mathbf{Z}+\frac{\mathbf{R}}{\rho}\right\|_F^2 \\ \text{s.t.} \quad & \operatorname{rank}(\mathbf{Z}) = 1. \end{aligned}$$

The problem $\bar{\mathcal{P}}_4^{\mathbf{Z}}$ can be solved using the SVD of $\mathbf{X}+\frac{\mathbf{R}}{\rho}$. Given the equation $\mathbf{X}+\frac{\mathbf{R}}{\rho} = \sum_{i=1}^{r}\sigma_i\mathbf{u}_i\mathbf{v}_i$ where r is the rank of the matrix $\mathbf{X}+\frac{\mathbf{R}}{\rho}$, σ_i are the singular values of $\mathbf{X}+\frac{\mathbf{R}}{\rho}$ ordered in nonincreasing form, $\mathbf{u}_i$ are the left-singular vectors of $\mathbf{X}+\frac{\mathbf{R}}{\rho}$, and $\mathbf{v}_i$ are the right-singular vectors of $\mathbf{X}+\frac{\mathbf{R}}{\rho}$, the closed-form solution for $\bar{\mathcal{P}}_4^{\mathbf{Z}}$ in the one-rank case is $\sigma_1\mathbf{u}_1\mathbf{v}_1$.

Algorithm 1 ASSD Method

Require: $\mathbf{A}_k = 0$, $\mathbf{B}$, λ, $\mathbf{x}^{(0)}$, η_{ADMM}, η_{D}
Ensure: A solution $\mathbf{x}_{\text{opt}}$ for $\bar{\mathcal{P}}_1$

Set $l = 0$, $q^{(0)} = 0$, $\mathbf{X}^{(l)} = \mathbf{x}^{(l)}\mathbf{x}^{(l)^H}$;
repeat
  $l \leftarrow l + 1$
  Convert $\bar{\mathcal{P}}_1$ to $\bar{\mathcal{P}}_1^q | q = q^{(l-1)}$ using the Dinkelbach method;
  Set $i = 0$
  repeat
    $i \leftarrow i + 1$
    Solve $\bar{\mathcal{P}}_4^{\mathbf{X},\alpha}$ to find the optimal value $\mathbf{X}_i^{(l)}$
    Solve $\bar{\mathcal{P}}_4^{\mathbf{Z}}$ based on SVD as mentioned in subsection updating $\mathbf{Z}$ to find the optimal values $\mathbf{Z}_i^{(l)}$
    Update $\mathbf{R}_i^{(l)}$ based on (22)
  until $|\mathbf{X}_i^{(l)} - \mathbf{Z}_i^{(l)}|F \leq \eta_{\text{ADMM}}$
  Inner Output: $\mathbf{X}^{(l)} = \mathbf{X}_i^{(l)}$
  Find the root of obj$(\bar{P}_1^q)$ with respect to q to obtain $q^{(l)}$
until $\left|q^{(l)} - q^{(l-1)}\right| \leq \eta_{\text{D}}$
Output: $\mathbf{x}_{\text{opt}} = \sqrt{\lambda_{\max}(\mathbf{X}^{(l)})} \cdot$ eigenvector corresponding to $\lambda_{\max}(\mathbf{X}^{(l)})$

4.1.3. Updating $\mathbf{R}$

In updating our Lagrange multiplier matrix $\mathbf{R}_i$, we use the results from updating $\mathbf{X}$ and $\mathbf{Z}$, denoted as $\mathbf{X}_i$ and $\mathbf{Z}_i$, respectively. This gives us:

$$\mathbf{R}_{i+1} = \mathbf{R}_i + \rho(\mathbf{X}_i - \mathbf{Z}_i). \tag{22}$$

According to the inner ADMM process we discussed, we need to continue iterating through $\mathbf{X}_i$, $\mathbf{Z}_i$, and $\mathbf{R}_i$ until the following stopping criterion is satisfied:

$$\|\mathbf{X}_i - \mathbf{Z}_i\|_F \leq \eta_{\text{ADMM}}. \tag{23}$$

For an overview of our proposed method, see Algorithm 1.

4.2. LSE-RCG Approach

With the closed-form expression of the objective function of $\bar{\mathcal{P}}_1$ at hand, manifold optimization is utilized to address the mentioned optimization problem. The geometrical structure of the manifold helps to avoid some saddle points and delivers high-quality solutions to our problem [23, 63, 64]. Essentially, a manifold generalizes Euclidean space and can only be locally approximated by a linear space around its points. The developed algorithm is a variant of the conjugate gradient algorithm, incorporating geometric operations for the conversion from Euclidean space to the manifold.

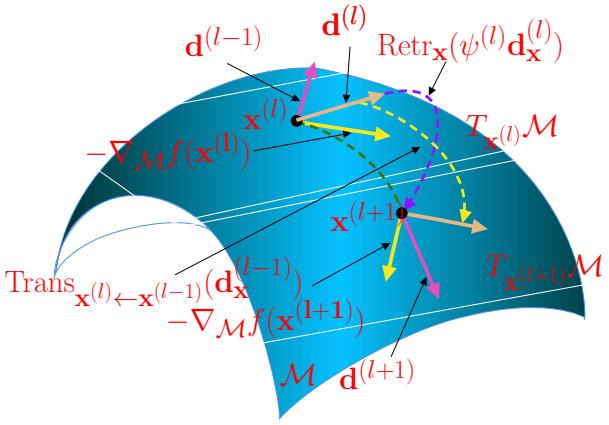

Figure 2: The geometric interpretation of Riemannian conjugate gradient descent (RCG).

Once more, let us consider $\bar{\mathcal{P}}_1^q$. When optimizing over $\mathbf{x}$, for $\gamma = 1$, the feasible region corresponds to $\|\mathbf{x}\|_2^2 = 1$, resembling a sphere manifold. However, when $\gamma = \frac{1}{N}$, the feasible region alters to $\|\mathbf{x}\|_2^2 = 1$ and $|x(n)| \leq \frac{1}{\sqrt{N}}$ for $n = 0, \ldots, N-1$, treating it as a complex circle manifold. By defining these manifolds, it is as if we are dealing with unconstrained optimization problems over these defined manifolds:

$$\text{for} \quad \gamma = 1: \quad \mathcal{M}_{\mathbf{x}} = \{\mathbf{x} \in \mathbb{C}^N \mid \|\mathbf{x}\|_2 = 1,\, i = 1, 2, \ldots, N\}, \tag{24}$$

$$\text{for} \quad \gamma = \frac{1}{N}: \quad \mathcal{M}_{\mathbf{x}} = \{\mathbf{x} \in \mathbb{C}^N \mid |x_i| = \frac{1}{\sqrt{N}},\, i = 1, 2, \ldots, N\}. \tag{25}$$

Smooth manifolds exhibit a property where they can be locally approximated by linear structures around every point. This local approximation at a point $\mathbf{x} \in \mathcal{M}_{\mathbf{x}}$ is referred to as the tangent space at $\mathbf{x}$. To be precise, the tangent space of $\mathcal{M}_{\mathbf{x}}$ at $\mathbf{x}^{(l)}$ consists of linear subspaces embedded within $\mathbb{C}^N$, and can be represented as:

$$\text{for} \quad \gamma = 1: T_{\mathbf{x}^{(l)}}\mathcal{M} = \{\boldsymbol{\xi} \in \mathbb{C}^N \mid \mathrm{Re}\{\boldsymbol{\xi}^H \mathbf{x}\} = 0\}, \tag{26}$$

$$\text{for} \quad \gamma = \frac{1}{N}: T_{\mathbf{x}^{(l)}}\mathcal{M} = \{\boldsymbol{\xi} \in \mathbb{C}^N \mid \mathrm{Re}\{\boldsymbol{\xi} \odot \mathbf{x}^*\} = 0\}. \tag{27}$$

Here, $\boldsymbol{\xi}$ represents a tangent vector situated at the point $\mathbf{x}^{(l)}$ within the tangent space $T_{\mathbf{x}^{(l)}}\mathcal{M}$.

Suppose we have converted our original max-min optimization problem $\bar{\mathcal{P}}_1^q$ into a minimization problem, where $f(\mathbf{x})$ acts as the objective function of the minimization problem (Details on this conversion will be provided in the following subsection.). To define the Riemannian gradient of $f(\mathbf{x})$ on our selected manifold $\mathcal{M}$, we first need to specify a Riemannian metric for $\mathcal{M}$. A convenient approach is to regard $\mathcal{M}$ as a Riemannian submanifold embedded within the Euclidean space $\mathbb{C}^N$ by equipping it with the induced Riemannian metric.

Hence, we can adopt the standard Euclidean inner product as our Riemannian metric:

$$\langle \boldsymbol{\xi}, \boldsymbol{\eta} \rangle = \mathrm{Re}\{\boldsymbol{\xi}^H \boldsymbol{\eta}\}, \tag{28}$$

where $\boldsymbol{\eta}$, similar to $\boldsymbol{\xi}$, represents tangent vectors at $\mathbf{x}^{(l)}$ on the tangent space $T_{\mathbf{x}^{(l)}}\mathcal{M}$, and the operator $\langle \cdot, \cdot \rangle$ in the following derivation is consistent with this Riemannian metric.

To advance, we define the Riemannian gradient $\nabla_{\mathcal{M}} f$ as the unique element within $T_{x^{(l)}}\mathcal{M}$ that leads to the steepest decrease of f:

$$\mathcal{D}f(\mathbf{x})[\boldsymbol{\xi}_{\mathbf{x}}] = g(\nabla_{\mathcal{M}} f(\mathbf{x}), \boldsymbol{\xi}_{\mathbf{x}}), \quad \forall \boldsymbol{\xi}_{\mathbf{x}} \in T_{\mathbf{x}}\mathcal{M}, \tag{29}$$

where $\mathcal{D}f(\mathbf{x})[\boldsymbol{\xi}_{\mathbf{x}}]$ is the directional derivative of $f(\mathbf{x})$ at $\mathbf{x}$ in the direction of $\boldsymbol{\xi}$. Since $\mathcal{M}_{\mathbf{x}}$ is submanifold of Euclidean space $\mathbb{C}^N$, we further have that $\nabla_{\mathcal{M}} f(\mathbf{x})$ is the orthogonal projection of the Euclidean gradient $\nabla f(\mathbf{x})$ to $T_{\mathbf{x}}\mathcal{M}_{\mathbf{x}}$, respectively:

$$\text{for} \quad \gamma = 1 : \nabla_{\mathcal{M}} f = \nabla f - \mathrm{Re}\{\mathbf{x}^H \nabla f\}\mathbf{x}, \tag{30}$$

$$\text{for} \quad \gamma = \frac{1}{N} : \nabla_{\mathcal{M}} f(\mathbf{x}) = \nabla f(\mathbf{x}) - \mathbf{x} \odot \mathrm{Re}(\nabla f(\mathbf{x}) \odot \mathbf{x}^*). \tag{31}$$

Given the concepts outlined above regarding the manifold, we embrace the RCG framework, a specialized variant of the conjugate gradient algorithm designed for Riemannian manifolds. Thanks to the local Euclidean structure present on $T_{\mathbf{x}^{(l)}}\mathcal{M}_{\mathbf{x}}$, the descent direction $\mathbf{d}^{(l)}$ is expressed as:

$$\mathbf{d}_{\mathbf{x}}^{(l)} = -\nabla_{\mathcal{M}} f(\mathbf{x}^{(l)}) + \mu_{\mathbf{x}}^{(l-1)} \mathrm{Trans}_{\mathbf{x}^{(l)} \leftarrow \mathbf{x}^{(l-1)}}(\mathbf{d}_{\mathbf{x}}^{(l-1)}), \tag{32}$$

where

$$\mathrm{Trans}_{\mathbf{x}^{(l)} \leftarrow \mathbf{x}^{(l-1)}}(\mathbf{d}_{\mathbf{x}}^{(l-1)}) = \mathrm{Proj}_{T_{\mathbf{x}^{(l)}}\mathcal{M}_{\mathbf{x}}}(\mathbf{d}_{\mathbf{x}}^{(l-1)}) \tag{33}$$

represents the transport operation that projects the tangent vector $\mathbf{d}_{\mathbf{x}}^{(l-1)} \in T_{\mathbf{x}}^{(l-1)}\mathcal{M}$ to $T_{\mathbf{x}}^{(l)}\mathcal{M}$. Specifically, for the manifold of the unit sphere and the complex circle manifold, the transport operators are obtained as

follows, respectively:

$$\text{for} \quad \gamma = 1: \quad \text{Trans}_{\mathbf{x}^{(l)} \leftarrow \mathbf{x}^{(l-1)}}(\mathbf{d}_{\mathbf{x}}^{(l-1)}) = \mathbf{d}_{\mathbf{x}}^{(l-1)} - \text{Re}\{\mathbf{x}^H \mathbf{d}_{\mathbf{x}}^{(l-1)}\}\mathbf{x}, \tag{34}$$

$$\text{for} \quad \gamma = \frac{1}{N}: \quad \text{Trans}_{\mathbf{x}^{(l)} \leftarrow \mathbf{x}^{(l-1)}}(\mathbf{d}_{\mathbf{x}}^{(l-1)}) = \mathbf{d}_{\mathbf{x}}^{(l-1)} - \mathbf{x}^{(l)} \odot \text{Re}\{\mathbf{d}_{\mathbf{x}}^{(l-1)} \odot \mathbf{x}^{(l)*}\}. \tag{35}$$

Here, $\mu^{(l-1)}$ represents the Polak-Ribière parameter [65], defined as:

$$\mu_{\mathbf{x}}^{(l-1)} = \frac{\langle \nabla_{\mathcal{M}} f(\mathbf{x}^{(l)}), \nabla_{\mathcal{M}} f(\mathbf{x}^{(l)}) - \text{Proj}_{T_{\mathbf{x}^{(l)}}\mathcal{M}}(\nabla f(\mathbf{x}^{(l-1)})) \rangle}{\langle \nabla_{\mathcal{M}} f(\mathbf{x}^{(l-1)}), \nabla_{\mathcal{M}} f(\mathbf{x}^{(l-1)}) \rangle}, \tag{36}$$

where $\text{Proj}_{T_{\mathbf{x}^{(l)}}\mathcal{M}}(\nabla f(\mathbf{x}^{(l-1)}))$ is obtained from (33).

To guarantee that the updated $\mathbf{x}^{(l+1)}$ moves in the direction of $\mathbf{d}_{\mathbf{x}}^{(l)}$ and stays within the confines of the manifold $\mathcal{M}$, we establish the retraction operator to map the tangent vector $\boldsymbol{\xi}_{\mathbf{x}} \in T_{\mathbf{x}^{(l)}}\mathcal{M}_{\mathbf{x}}$ back to the manifold $\mathcal{M}_{\mathbf{x}}$, as follows:

$$\text{for} \quad \gamma = 1: \text{Retr}_{\mathbf{x}}(\boldsymbol{\xi}_{\mathbf{x}}) = \frac{\mathbf{x} + \boldsymbol{\xi}_{\mathbf{x}}}{\|\mathbf{x} + \boldsymbol{\xi}_{\mathbf{x}}\|}, \tag{37}$$

$$\text{for} \quad \gamma = \frac{1}{N}: \text{Retr}_{\mathbf{x}}(\boldsymbol{\xi}_{\mathbf{x}}) = (\mathbf{x} + \boldsymbol{\xi}_{\mathbf{x}}) \odot \frac{1}{|\mathbf{x} + \boldsymbol{\xi}_{\mathbf{x}}|}. \tag{38}$$

Thus, the updated $\mathbf{x}^{(l+1)}$ is retracted to the manifold by:

$$\mathbf{x}^{(l+1)} = \text{Retr}_{\mathbf{x}}(\psi^{(l)} \mathbf{d}_{\mathbf{x}}^{(l)}), \tag{39}$$

where $\psi^{(l)}$ is the step size determined by the following backtracking Armijo line-search method [66]:

$$\psi^{(l)} = \beta^j \alpha,$$

$$f(\mathbf{x}^{(l)}) - f(\text{Retr}_{\mathbf{x}}(\psi^{(l)} \mathbf{d}_{\mathbf{x}}^{(l)})) \geq -\delta \langle \nabla f(\mathbf{x}^{(l)}), \psi^{(l)} \mathbf{d}_{\mathbf{x}}^{(l)} \rangle. \tag{40}$$

Here, $\alpha > 0$, β and δ lie within the interval $(0, 1)$, and j denotes the smallest non-negative integer that meets the stated condition. Figure 2 provides a clear visualization of the RCG algorithm during each iteration.

As previously mentioned, to derive the Riemannian gradient from the objective function, we require a closed form of the objective function. Therefore, we aim to rephrase problem $\bar{\mathcal{P}}_1$ in the following manner.

4.2.1. Log-sum-exp approximation

In this part, our goal is to apply the RCG approach to a distinct approximation of our objective function. Let us revisit $\bar{\mathcal{P}}_1^q$. Utilizing

$$\max_{\mathbf{x}} \min_{k} \mathbf{x}^H \mathbf{C}_k \mathbf{x} = -\min_{\mathbf{x}} \max_{k} -\mathbf{x}^H \mathbf{C}_k \mathbf{x}, \tag{41}$$

$$\arg\max_{\mathbf{x}} \min_{k} \mathbf{x}^H \mathbf{C}_k \mathbf{x} = \arg\min_{\mathbf{x}} \max_{k} -\mathbf{x}^H \mathbf{C}_k \mathbf{x}, \tag{42}$$

we arrive at the modified optimization problem:

$$\begin{aligned} \bar{\mathcal{P}}_2^q : \quad & \min_{\mathbf{x}} \max_{k} \quad -\mathbf{x}^H \mathbf{C}_k \mathbf{x} \\ & \text{s.t.} \quad \mathbf{x} \in \mathcal{M}_{\mathbf{x}}. \end{aligned} \tag{43}$$

Given that the maximum of a function can be approximated using the log-sum-exp function, our optimization problem transforms into:

$$\begin{aligned} \bar{\mathcal{P}}_2^q : \quad & \min_{\mathbf{x}} \quad \epsilon \ln \sum_{k=1}^{K} \exp\left(\frac{-\mathbf{x}^H \mathbf{C}_k \mathbf{x}}{\epsilon}\right) \\ & \text{s.t.} \quad \mathbf{x} \in \mathcal{M}_{\mathbf{x}}. \end{aligned} \tag{44}$$

For a much more precise approximation, we should select the scaling factor ϵ to be as small as possible. To transition from the Euclidean gradient to the Riemannian gradient descent, we express the Euclidean gradient as:

$$\nabla f(\mathbf{x}^{(l)}) = -2 \sum_{k=1}^{K} \frac{\exp(-\mathbf{x}^{(l)T} \mathbf{C}_k \mathbf{x}^{(l)})}{\sum_{j=1}^{K} \exp(-\mathbf{x}^{(l)T} \mathbf{C}_j \mathbf{x}^{(l)})} \mathbf{C}_k \mathbf{x}^{(l)}. \tag{45}$$

For a detailed description of the approach used to solve $\tilde{\boldsymbol{P}}_3$ with the log-sum-exp-based method (known as the LSE-RCG method), please see Algorithm 2.

4.3. Computational Complexity of ASSD and LSE-RCG

In this paper, the ASSD method tackles each of $\mathcal{P}_{\mathbf{w}}^{(m)}$ and $\mathcal{P}_{\mathbf{s}}^{(m)}$ by first employing the Dinkelbach method and then applying ADMM. This method divides the problem into a SDP problem and a fixed-rank non-convex optimization problem. The SDP part of $\mathcal{P}_{\mathbf{w}}^{(m)}$ has a complexity of $O(N^{6.5})$, while the SDP part of $\mathcal{P}_{\mathbf{s}}^{(m)}$ has a complexity of $O(M^{6.5})$. For the fixed-rank part, which has the advantage of being solved in one iteration, $\mathcal{P}_{\mathbf{w}}^{(m)}$ has a complexity of $O(M^3)$ and $\mathcal{P}_{\mathbf{s}}^{(m)}$ has a complexity of $O(N^3)$.

To evaluate the complexity of the LSE-RCG Algorithm, we focus on the log-sum-exp part, the most com-

Algorithm 2 LSE-RCG algorithm

Consider an initial $x^{(0)}$, tolerance parameter $\epsilon > 0$, and set $l = 0$;
Calculate $\mathbf{d}_{\mathbf{x}}^{(l)} = -\nabla_{\mathcal{M}} f$ according to (30) or (31), depending on whether dealing with the sphere manifold or the complex circle manifold.
Choose Armijo backtracking line search step size $\psi^{(l)}$ according to (40);
repeat
    $l \leftarrow l + 1$;
    Find the point $\mathbf{x}^{(l)}$ using retraction in (39);
    Determine Riemannian gradient $\nabla_{\mathcal{M}} f$ according to (30) or (31), depending on whether dealing with the sphere manifold or the complex circle manifold;
    Calculate the vector transport $\text{Trans}_{\mathbf{x}^{(l)} \leftarrow \mathbf{x}^{(l-1)}}(\mathbf{d}_{\mathbf{x}}^{(l-1)})$ according to (34) or (35), depending on whether dealing with the sphere manifold or the complex circle manifold;
    Obtain Polak-Ribiere parameter $\mu^{(l-1)}$ according to (36);
    Compute conjugate search direction $\mathbf{d}_{\mathbf{x}}^{(l)}$ with (32);
    Choose Armijo backtracking line search step size $\psi^{(l)}$ according to (40);
until $\|\nabla_{\mathcal{M}} f\|_2 \leq \epsilon$.

putationally demanding component. Each matrix-vector multiplication $\mathbf{C}_i \mathbf{x}^{(l)}$ and quadratic form $\mathbf{x}^{(l)T} \mathbf{C}_i \mathbf{x}^{(l)}$ requires $O((\text{length}(\mathbf{x}))^2)$ operations. The inner summation over j in the denominator involves K terms, each requiring a quadratic form computation, resulting in $O(K \cdot (\text{length}(\mathbf{x}))^2)$. Similarly, the outer summation over i and the subsequent multiplication add another $O(K \cdot (\text{length}(\mathbf{x}))^2)$. Accordingly, each update of $\mathcal{P}_{\mathbf{w}}^{(m)}$ has a complexity of $O(K \cdot M^2)$, and each update of $\mathcal{P}_{\mathbf{s}}^{(m)}$ has a complexity of $O(K \cdot N^2)$.

5. Numerical Results

Let us delve into the assessment of the proposed method using the available TIR information. We will explore its effectiveness across various scenarios, considering the uncertainty associated with the TIR data. Our focus is on an S-band radar with specific parameters: a rectangular subpulse duration of 6.67 ns and a working frequency of $f_c = 3$ GHz, resulting in an approximate range resolution of 1 meter.

To model the TIR of extended targets, we generate radar backscattering data using simulation software referenced in [67, 68]. Specifically, we simulate data for two different aircraft: the F15 and the Tornado. The F-15 has target dimensions of 19.43 meters in length and 13.05 meters in width, while the Tornado measures 16.72 meters in length and 13.91 meters in width.Considering the targets' dimensions and the radar's range resolution, we define the TIR support interval as $Q = 17$.

Let us explore the statistical properties of the clutter environment and noise. In our scenario, we consider a

homogeneous clutter environment where the elements of the covariance matrix follow an exponential distribution:

$$R_c(n,n') = \sigma_c^2 r^{-|n-n'|}, \quad (n,n') \in \{1,...,M+N\}^2. \tag{46}$$

Here, we set $\sigma_c^2 = 10$ and $r = 0.8$. As to the noise, we suppose a discrete white noise with variance $\sigma_{\boldsymbol{\upsilon}}^2 = 1$. Regarding the parameter configurations and stopping criteria for our proposed methods, we set $\rho = 2$ and $\eta_{\text{ADMM}} = 10^{-4}$ for the ASSD method. Moreover, for the ADMM within ASSD, whether for updating $\mathbf{s}$ or for updating $\mathbf{w}$, the initial values of $\mathbf{Z}$ and $\mathbf{R}$ are considered as zero matrices. Additionally, the LSE-RCG method uses a scaling factor $\epsilon = 10^{-4}$. Furthermore, both proposed methods are configured with $\eta = 10^{-4}$.

Regarding the initial value for the transmit waveform $\mathbf{s}$, we first consider the transmit waveform as a sequence with linear frequency modulation (LFM) to satisfy condition (11) related to signal energy:

$$s_0(n) = \frac{1}{\sqrt{N}} e^{j\pi \frac{n^2}{2N}}, \quad n = 0, 1, \ldots, N-1. \tag{47}$$

Then, to obtain the initial value for the receiver filter $\mathbf{w}$, we use the initial value $\mathbf{s}$ obtained by (47) to create $\mathbf{S} = \mathbf{s}\mathbf{s}^H$. By substituting this into the optimization problem (17) and defining $\mathbf{W} = \mathbf{w}\mathbf{w}^H$, we reformulate the problem as an SDP by relaxing the rank-one constraint, as shown below:

$$\begin{aligned} \max_{\mathbf{W},\alpha} \quad & \alpha \\ \text{s.t.} \quad & \operatorname{tr}\left(\boldsymbol{\Sigma}_{\mathbf{C}\boldsymbol{\upsilon}}(\mathbf{S})\mathbf{W}\right) = 1 \\ & \operatorname{tr}\left(\boldsymbol{\Gamma}(\mathbf{T}_i, \mathbf{S})\mathbf{W}\right) \geq \alpha, \\ & \mathbf{W} \succeq 0. \end{aligned} \tag{48}$$

After obtaining the optimal value $\mathbf{W}$ from (48), we consider the initial value for the receiver filter $\mathbf{w}$ as $\sqrt{\lambda_1}\mathbf{v}_1$, where λ_1 is the maximum eigenvalue of $\mathbf{W}$ and $\mathbf{v}_1$ is the corresponding eigenvector. Next, we substitute the receiver filter $\mathbf{w}$ into the following optimization problem:

$$
\begin{aligned}
\max_{\mathbf{S},\alpha} \quad & \alpha \\
\text{s.t.} \quad & \operatorname{tr}\left(\bar{\mathbf{\Sigma}}_{\mathbf{C}\boldsymbol{\upsilon}}(\mathbf{W})\mathbf{S}\right) = 1 \\
& \operatorname{tr}\left(\bar{\mathbf{\Gamma}}(\mathbf{T}_i, \mathbf{W})\mathbf{S}\right) \geq \alpha, \\
& \operatorname{tr}(\mathbf{E}_n\mathbf{X}) \leq \frac{1}{N}, \\
& \mathbf{S} \succeq 0.
\end{aligned} \tag{49}
$$

After solving this optimization problem, we obtain the initial value for $\mathbf{s}$ as $\sqrt{\bar{\lambda}_1}\bar{\mathbf{v}}_1$, where $\bar{\lambda}_1$ is the maximum eigenvalue of $\mathbf{S}$ and $\bar{\mathbf{v}}_1$ is the corresponding eigenvector. It is worth mentioning that this $\mathbf{s}$ is then used as the initial value for our ASSD algorithm, not the one from (47).

Now, our objective is to assess the effectiveness of the proposed methods in jointly designing the transmit signal and receive filter under the constant modulus condition. We will investigate three distinct scenarios, as outlined below:

1. Iteration-based convergence: Evaluating the speed of convergence by counting the iterations needed.
2. Influence of diverse TAA uncertainty sets on SINR and convergence: We investigate the effects of different TAA uncertainty sets on both SINR and convergence for a specified target.
3. Influence of different target types with unique TAA uncertainty sets: Examining how different target types, each with their own TAA uncertainty sets, affect the results.

Considering the uncertainty set, we configured the TAA sampling step for $\mathcal{I}_{\phi_1}^{\phi_2}$ to 0.1 degrees in our simulations. For each TAA $k\Delta\theta$ within this uncertainty set, we calculate the actual TIR using the toolbox cited in [67, 68].

To validate the effectiveness of our approach, we compare the optimized SINR achieved by our method against those obtained from other waveform-filter design techniques. The first comparison is with a simplified version of the unconstrained design method from [22], which assumes knowledge of the TIR and is specifically designed for SISO scenarios. We also consider the manifold-based nominal method from [23, 24], which, like [22], assumes exact TIR knowledge and incorporates a constant modulus constraint. This method defines a complex circle manifold and uses Riemannian conjugate gradient descent for the design of waveform-filter pairs. Lastly, we evaluate the nominal and robust design method from [25], which employs a constant modulus constraint as a PAR constraint, accounts for TIR uncertainties (only in the robust design), and employs randomization

strategies to generate waveform-filter pairs after solving a relaxed version of the problem.

5.1. The Optimal SINR Obtained for Different TAAs

Figure (3) displays the worst-case $\text{SINR}^{(m)}$ against iteration m for various design strategies. For comparison with the robust method described in [25], their worst-case SINR versus iteration has been plotted in such a way that randomization is applied after the last iteration. For instance, the curve at $m = 5$ represents a scenario in which 4 iterations are conducted without randomization, and randomization is applied only after the 5^{th} iteration when updating $(\mathbf{s}, \mathbf{w})$. The non-monotonic behavior observed in the robust approach of [25] can be attributed to their randomization stage, where they aim to pick only 50 random samples (as mentioned in their paper). To prevent their approach from becoming slower and to ensure a fair comparison, we have kept this parameter exactly as described in their paper. For comparison, we considered three uncertainty sets: $\mathcal{I}^{3^\circ}_{-3^\circ}$, $\mathcal{I}^{4^\circ}_{-4^\circ}$, and $\mathcal{I}^{5^\circ}_{-5^\circ}$. The plots clearly show that as the uncertainty set size increases, our approach yields lower worst-case SINR values. This conforms with the principle that for two sets of uncertainties $\mathcal{I}_1$ and $\mathcal{I}_2$ where $\mathcal{I}_1 \subseteq \mathcal{I}_2$, the minimum SINR over $\mathcal{I}_2$ is less than or equal to that over $\mathcal{I}_1$. Hence, solutions with larger uncertainty sets tend to have worse worst-case SINR values.

In a separate analysis, we present the SINR achieved against the TAA within the uncertainty set considered during the design phase (refer to Fig. 4). It is worth noting that the nominal design approaches proposed in [25], along with the manifold-based nominal method from [23, 24], optimize SINR specifically for the matched TAA $\mathcal{I}^{0^\circ}_{0^\circ}$. In contrast, the robust design from [25] and our proposed approaches focus on optimizing the worst-case SINR across the predefined uncertainty set. This comparison is carried out over the uncertainty sets $\mathcal{I}^{3^\circ}_{-3^\circ}$, $\mathcal{I}^{4^\circ}_{-4^\circ}$, and $\mathcal{I}^{5^\circ}_{-5^\circ}$. As previously mentioned, the plots illustrate that enlarging the TAA uncertainty set results in reduced worst-case SINR values. Furthermore, the findings indicate that both the ASSD and LSE-RCG approaches demonstrate superior performance in terms of minimum SINR values and, as a result, exhibit more robust SINR values over the entire TAA uncertainty set compared to all competitor methods, especially its main competitor [25], which served as the benchmark before the introduction of our proposed solutions.

5.2. The Performance of SINR for a Different Target

In this subsection, we evaluate the performance of the proposed method for a different target type—specifically, the Tornado—within the uncertainty set $\mathcal{I}^{3^\circ}_{-3^\circ}$ (see Fig. 5). This analysis is conducted in a manner similar to our evaluation of the F15 target (see Fig. 4). As observed, the proposed method in [22], the manifold-based method from [23, 24], and the nominal method from [25] exhibit inferior performance due to their inability to account for worst-case scenarios within the uncertainty set. In contrast, the ASSD and LSE-RCG approaches

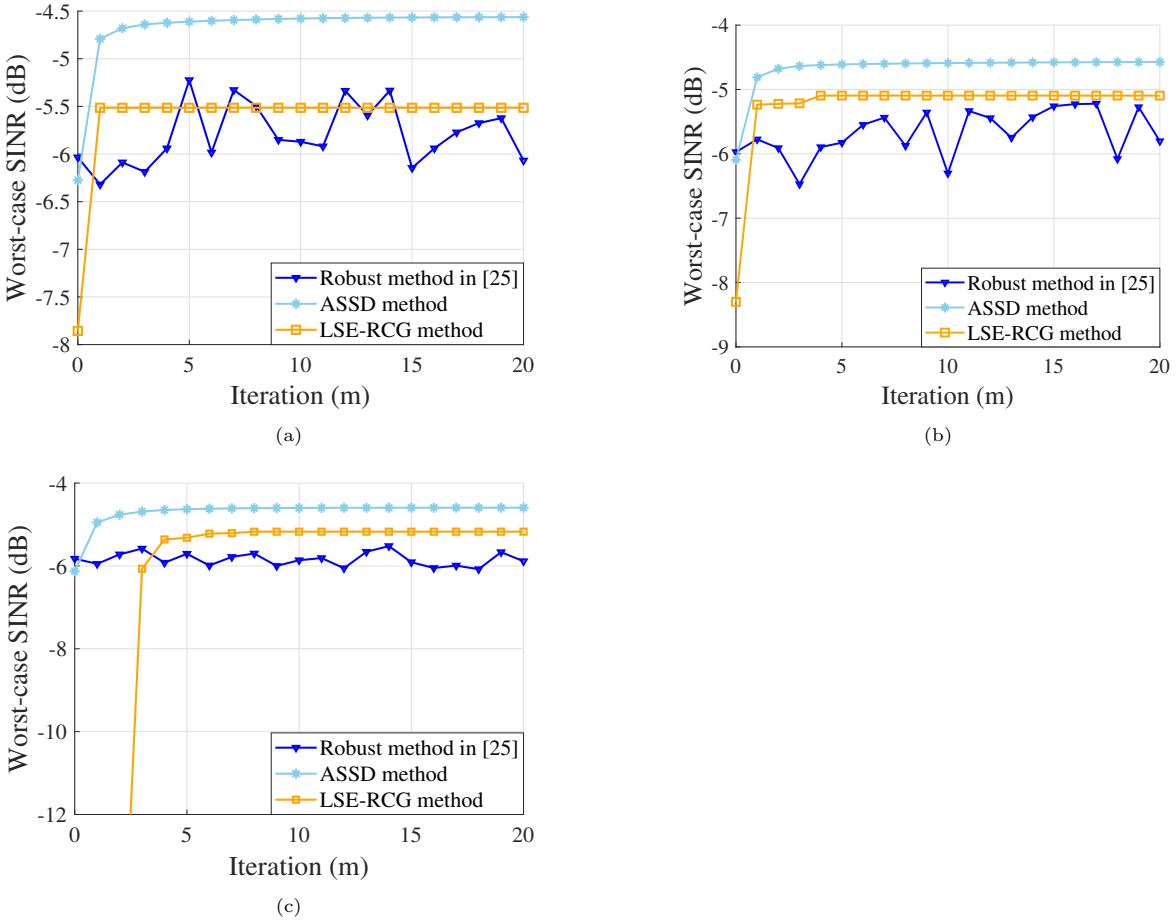

Figure 3: Plotting $\text{SINR}^{(m)}$ versus the Number of Iterations for the F15 Target, considering three different TAA uncertainty sets: (a) $\mathcal{I}^{3^\circ}_{-3^\circ}$, (b) $\mathcal{I}^{4^\circ}_{-4^\circ}$, (c) $\mathcal{I}^{5^\circ}_{-5^\circ}$.

demonstrate superior performance, achieving higher SINR values across the entire TAA uncertainty set and surpass other methods, especially the robust method proposed by [25], in terms of attaining higher minimum SINR values.

5.3. Execution time

As the final examination, we evaluate the performance of the methods based on their execution times. Refer to Table 1, which presents the convergence times of our approaches in seconds, compared to the method proposed by [22], the manifold-based methods in [23, 24], and the nominal and robust methods from [25]. As shown, the LSE-RCG method demonstrates the lowest runtime, showcasing significant superiority in convergence time. Although the ASSD method ranks behind the robust method from [25] in terms of execution time, it was observed in the previous two subsections that ASSD achieved the best accuracy by attaining the highest minimum SINR.

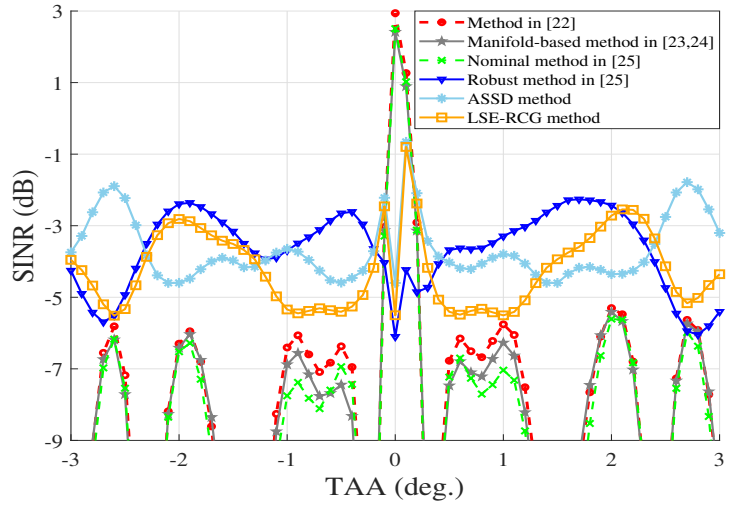

(a)

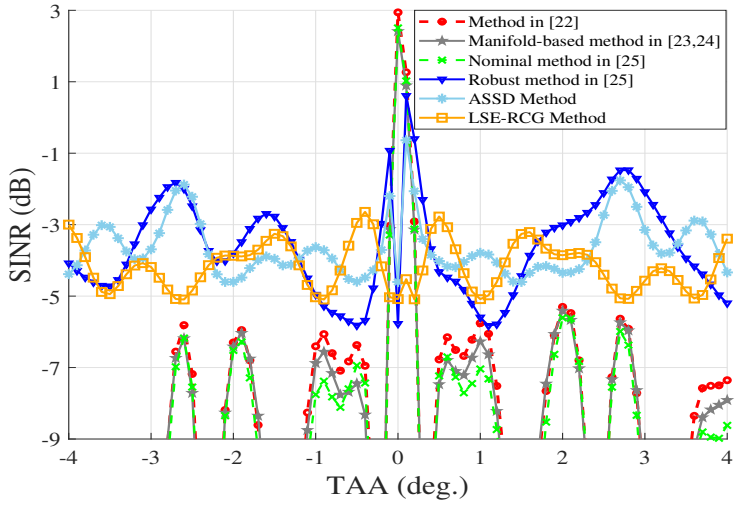

(b)

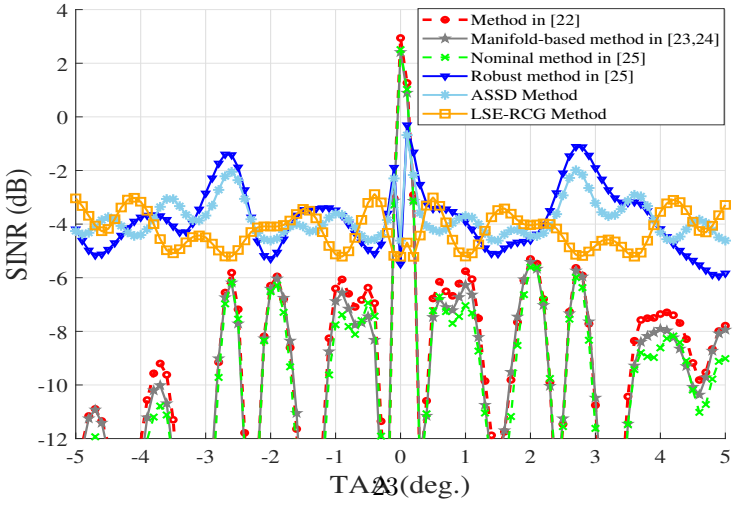

(c)

Figure 4: SINR versus TAA, over different uncertainty sets for F15: (a) $\mathcal{I}^{3^\circ}_{-3^\circ}$, (b) $\mathcal{I}^{4^\circ}_{-4^\circ}$, (c) $\mathcal{I}^{5^\circ}_{-5^\circ}$.

It is worth noting that, although the runtimes of the method in [22], the manifold-based methods in [23, 24], and the nominal method in [25] are extremely low, these methods are not of interest because they only consider the matched situation ($\mathcal{I}_{0^\circ}^{0^\circ}$) and do not account for the uncertainty sets of TAA.

Table 1: Examining runtime performance (in seconds) across different uncertainty sets and target types.

Algorithm	$\mathcal{I}_{-3^\circ}^{3^\circ}$ (F15)	$\mathcal{I}_{-4^\circ}^{4^\circ}$ (F15)	$\mathcal{I}_{-5^\circ}^{5^\circ}$ (F15)	$\mathcal{I}_{-3^\circ}^{3^\circ}$ (Tornado)
Method in [22]	0.5394	0.5375	0.4902	0.4115
Manifold-based method in [23, 24]	0.4362	0.297012	0.2903	0.2683
Nominal method [25]	14.9021	14.0891	14.1367	14.1727
Robust method [25]	46.7248	51.9721	55.8607	47.9586
ASSD method	63.4694	69.8073	77.6814	86.7538
LSE-RCG method	0.8432	1.1553	2.0650	1.3445

6. Conclusion

In this research, the challenge of optimizing the SINR for extended targets amidst signal-dependent interference has been addressed through the joint optimization of transmit codes and receive filters. To manage uncertainties related to the TIR, we introduced a worst-case optimization framework over a predefined uncertainty set, which comprises TIR samples corresponding to TAAs. This has led to a worst-case non-convex optimization problem. Additionally, our strategy incorporates a constant modulus constraint on the transmit code to ensure operation near transmitter saturation for radar systems. In this paper, we propose two approaches that employ a sequential optimization process to jointly design the transmit waveform and receive filter.

In the first approach, which we named ASSD, each design problem was decomposed using ADMM into an SDP problem and an non-convex problem due to a fixed rank constraint, solvable via singular value decomposition (SVD). The second approach tackled the problem over two Riemannian manifolds: the sphere manifold for the receive filter and the product of complex circles for the transmit signal. Manifold optimization treated the constrained problem as an unconstrained one within a restricted search space. We first converted our max-min problem into a min problem, resulting in a closed form of log-sum-exp. We then solved the reformulated problem using the Riemannian conjugate gradient descent algorithm, which was developed based on Euclidean conjugate gradient descent, leveraging specific properties of the manifold such as the Riemannian metric and retraction. We called this approach log-sum-exp RCG (LSE-RCG).

Our proposed methods offer significant advantages, including rapid convergence with minimal iterations, and one of our approaches is the fastest in runtime as well, which are particularly valuable in real-time applications

where swift decision-making is crucial. Furthermore, our approaches have not only improved SINR but also done so under worst-case scenarios, outperforming prior methods.

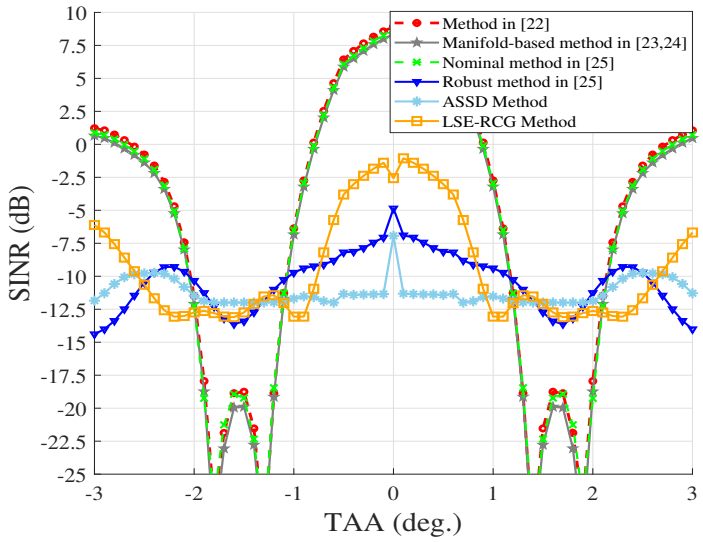

(a)

Figure 5: SINR versus TAA, over the uncertainty set $\mathcal{I}^{3^\circ}_{-3^\circ}$ for Tornado.

Appendix

A. The Proof of The SINR Formulation:

To prove how we arrive at the numerators in (12), consider the following:

$$\begin{aligned}\left|\mathbf{w}^H\mathbf{T}_\theta\mathbf{s}\right|^2 &= \mathbf{w}^H\mathbf{T}_\theta\mathbf{s}\mathbf{s}^H{\mathbf{T}_\theta}^H\mathbf{w} = \mathbf{w}^H\mathbf{\Gamma}(\mathbf{T}_\theta,\mathbf{S})\mathbf{w}\\ &= \mathbf{s}^H{T_\theta}^H\mathbf{w}\mathbf{w}^H\mathbf{T}_\theta\mathbf{s} = \mathbf{s}^H\bar{\mathbf{\Gamma}}(\mathbf{T}_\theta,\mathbf{W})\mathbf{s}.\end{aligned} \tag{50}$$

In order to prove the denominator part of (12), we simplify the denominator of (9) as follows:

$$\begin{aligned}\mathbb{E}[\left|\mathbf{w}^H\mathbf{C}\mathbf{s}\right|^2] + \mathbb{E}[\left|\mathbf{w}^H\boldsymbol{\upsilon}\right|^2] &= \mathbf{w}^H\mathbb{E}[\mathbf{C}\mathbf{s}\mathbf{s}^H\mathbf{C}^H]\mathbf{w} + \mathbf{w}^H\mathbb{E}[\boldsymbol{\upsilon}^H\boldsymbol{\upsilon}]\mathbf{w}\\ &= \mathbf{w}^H\mathbb{E}[\mathbf{C}\mathbf{s}\mathbf{s}^H\mathbf{C}^H]\mathbf{w} + \sigma^2_{\boldsymbol{\upsilon}}\mathbf{w}^H\mathbf{w}\\ &= \mathbf{w}^H\mathbf{\Sigma}_{\mathbf{C}\boldsymbol{\upsilon}}(\mathbf{S})\mathbf{w}.\end{aligned}$$

Considering the considered energy constraint, i.e. $\|\mathbf{s}\|_2^2 = 1$, the denominator of (9) becomes simpler:

$$\begin{aligned}\mathbb{E}[\left|\mathbf{w}^H\mathbf{C}\mathbf{s}\right|^2] + \mathbb{E}[\left|\mathbf{w}^H\boldsymbol{\upsilon}\right|^2] &= \mathbf{s}^H\mathbb{E}[\mathbf{C}\mathbf{w}\mathbf{w}^H\mathbf{C}^H]\mathbf{s} + \mathbf{w}^H\mathbb{E}[\boldsymbol{\upsilon}^H\boldsymbol{\upsilon}]\mathbf{w} \\ &= \mathbf{s}^H\mathbb{E}[\mathbf{C}\mathbf{w}\mathbf{w}^H\mathbf{C}^H]\mathbf{s} + \sigma_{\boldsymbol{\upsilon}}^2\mathrm{tr}(\mathbf{w}\mathbf{w}^H) \\ &= \mathbf{s}^H\bar{\boldsymbol{\Sigma}}_{\mathbf{C}\boldsymbol{\upsilon}}(\mathbf{W})\mathbf{s}.\end{aligned}$$

B. The Proof of Proposition 1

Firstly, we demonstrate that the sequence $\left\{\mathrm{SINR}^{(m)}\right\}$ is monotonically increasing, meaning $\mathrm{SINR}^{(m)} \leq \mathrm{SINR}^{(m+1)}$. To show this, we consider:

$$\begin{aligned}\mathrm{SINR}^{(m)} &= \min_{\theta\in\mathcal{I}} \frac{\mathrm{tr}\left(\boldsymbol{\Gamma}\left(\mathbf{T}_\theta, \mathbf{S}^{(m)}\right)\mathbf{W}^{(m)}\right)}{\mathrm{tr}\left(\boldsymbol{\Sigma}_{cv}\left(\mathbf{S}^{(m)}\right)\mathbf{W}^{(m)}\right)} \leq v\left(\mathcal{P}_{\mathbf{w}}^{(m+1)}\right) \\ &= \min_{\theta\in\mathcal{I}} \frac{\mathrm{tr}\left(\bar{\boldsymbol{\Gamma}}\left(\mathbf{T}_\theta, \mathbf{W}^{(m+1)}\right)\mathbf{S}^{(m)}\right)}{\mathrm{tr}\left(\bar{\boldsymbol{\Sigma}}_{cv}\left(\mathbf{W}^{(m+1)}\right)\mathbf{S}^{(m)}\right)} \leq v\left(\mathcal{P}_{\mathbf{s}}^{(m+1)}\right) \\ &= \mathrm{SINR}^{(m+1)}.\end{aligned}$$

Secondly, we need to show that the objective function is bounded above. We start with:

$$\begin{aligned}\mathrm{SINR}^{(m)} &= \min_{\theta\in\mathcal{I}} \frac{\mathrm{tr}\left(\bar{\boldsymbol{\Gamma}}\left(\mathbf{T}_\theta, \mathbf{W}^{(m)}\right)\mathbf{S}^{(m)}\right)}{\mathrm{tr}\left(\bar{\boldsymbol{\Sigma}}_{cv}\left(\mathbf{W}^{(m)}\right)\mathbf{S}^{(m)}\right)} \\ &\leq \min_{\theta\in\mathcal{I}} \frac{\mathrm{tr}\left(\mathbf{T}_\theta^H\mathbf{W}^{(m)}\mathbf{T}_\theta\mathbf{S}^{(m)}\right)}{\sigma_v^2\,\mathrm{tr}\left(\mathbf{W}^{(m)}\right)\mathrm{tr}\left(\mathbf{S}^{(m)}\right)} \\ &= \min_{\theta\in\mathcal{I}} \frac{\mathrm{tr}\left(\mathbf{T}_\theta\mathbf{S}^{(m)}\mathbf{T}_\theta^H\mathbf{W}^{(m)}\right)}{\sigma_v^2\,\mathrm{tr}\left(\mathbf{W}^{(m)}\right)} \qquad (51) \\ &\leq \min_{\theta\in\mathcal{I}} \frac{\mathrm{tr}\left(\mathbf{T}_\theta\mathbf{S}^{(m)}\mathbf{T}_\theta^H\right)\mathrm{tr}\left(\mathbf{W}^{(m)}\right)}{\sigma_v^2\,\mathrm{tr}\left(\mathbf{W}^{(m)}\right)} \qquad (52) \\ &\leq \min_{\theta\in\mathcal{I}} \frac{\mathrm{tr}\left(\mathbf{S}^{(m)}\right)\mathrm{tr}\left(\mathbf{T}_\theta^H\mathbf{T}_\theta\right)}{\sigma_v^2} \qquad (53) \\ &= \frac{N}{\sigma_v^2}\min_{\theta\in\mathcal{I}}\|\mathbf{h}_\theta\|^2.\end{aligned}$$

In the first inequality, we used (16) to state:

$$\bar{\boldsymbol{\Sigma}}_{cv}\left(\mathbf{W}^{(m)}\right) \succeq \sigma_v^2\,\mathrm{tr}\left(\mathbf{W}^{(m)}\right)\mathbf{I},$$

which leads to (51) because $\mathrm{tr}\left(\mathbf{S}^{(m)}\right) = 1$. Additionally, we employed the fact that for $\mathbf{A}, \mathbf{B} \succeq \mathbf{0}$:

$$0 \leq \mathrm{tr}(\mathbf{AB}) \leq \mathrm{tr}(\mathbf{A})\,\mathrm{tr}(\mathbf{B}),$$

to derive (52) and (53). Finally, $\mathrm{tr}\left(\mathbf{T}_\theta^H \mathbf{T}_\theta\right)$ represents the sum of the squared norms of the columns of $\mathbf{T}_\theta$. Considering the structure of $\mathbf{T}_\theta$, this can be expressed as $\mathrm{tr}\left(\mathbf{T}_\theta^H \mathbf{T}_\theta\right) = N \left\|\mathbf{h}_\theta\right\|_2^2$. Therefore, the upper bound on the sequence $\mathrm{SINR}^{(m)}$ is:

$$\mathrm{SINR}^{(m)} \leq \frac{N}{\sigma_v^2} \min_{\theta \in \mathcal{I}} \left\|\mathbf{h}_\theta\right\|_2^2 . \tag{54}$$

Under the finite energy assumption for the TIR, inequality (54) together with the monotonic increasing property of $\left\{\mathrm{SINR}^{(m)}\right\}$ guarantees the convergence of the objective function sequence.

References

[1] M. Bell, "Information theory and radar waveform design," *IEEE Transactions on Information Theory*, vol. 39, no. 5, pp. 1578–1597, 1993.

[2] W. Yuxi, H. Guoce, and L. Wei, "Waveform design for radar and extended target in the environment of electronic warfare," *Journal of Systems Engineering and Electronics*, vol. 29, no. 1, pp. 48–57, 2018.

[3] R. A. Romero and N. A. Goodman, "Waveform design in signal-dependent interference and application to target recognition with multiple transmissions," *IET radar, sonar & navigation*, vol. 3, no. 4, pp. 328–340, 2009.

[4] S. Pillai, D. Youla, H. Oh, and J. Guerci, "Optimum transmit-receiver design in the presence of signal-dependent interference and channel noise," in *Conference Record of the Thirty-Third Asilomar Conference on Signals, Systems, and Computers (Cat. No.CH37020)*, vol. 2, 1999, pp. 870–875 vol.2.

[5] S. P. Sira, Y. Li, A. Papandreou-Suppappola, D. Morrell, D. Cochran, and M. Rangaswamy, "Waveform-agile sensing for tracking," *IEEE Signal Processing Magazine*, vol. 26, no. 1, pp. 53–64, 2009.

[6] L. Wu, P. Babu, and D. P. Palomar, "Transmit waveform/receive filter design for MIMO radar with multiple waveform constraints," *IEEE Transactions on Signal Processing*, vol. 66, no. 6, pp. 1526–1540, 2018.

[7] S. M. Sowelam and A. H. Tewfik, "Optimal waveform selection for target classification," in *1996 8^{th} European Signal Processing Conference (EUSIPCO 1996)*, 1996, pp. 1–4.

[8] Z. Xu, Z. Xie, C. Fan, and X. Huang, "Probabilistically robust radar waveform design for extended target detection," *IEEE Transactions on Signal Processing*, vol. 70, pp. 4212–4224, 2022.

[9] B. Friedlander, "Waveform design for MIMO radars," *IEEE Transactions on Aerospace and Electronic Systems*, vol. 43, no. 3, pp. 1227–1238, Jul. 2007.

[10] A. Aubry, A. De Maio, and Y. Huang, "MIMO radar beampattern design via PSL/ISL optimization," *IEEE Transactions on Signal Processing*, vol. 64, no. 15, pp. 3955–3967, 2016.

[11] G. Cui, A. D. Maio, A. Farina, and J. Li, Eds., *Radar Waveform Design Based on Optimization Theory*, ser. Radar, Sonar and Navigation. Institution of Engineering and Technology, 2020.

[12] M. Bell, "Information theory and radar waveform design," *IEEE Transactions on Information Theory*, vol. 39, no. 5, pp. 1578–1597, 1993.

[13] Y. Yang and R. S. Blum, "MIMO radar waveform design based on mutual information and minimum mean-square error estimation," *IEEE Transactions on Aerospace and Electronic Systems*, vol. 43, no. 1, pp. 330–343, Jan. 2007.

[14] ——, "Minimax robust MIMO radar waveform design," *IEEE Journal of Selected Topics in Signal Processing*, vol. 1, no. 1, pp. 147–155, Jun. 2007.

[15] N. A. Goodman, P. R. Venkata, and M. A. Neifeld, "Adaptive waveform design and sequential hypothesis testing for target recognition with active sensors," *IEEE Journal of Selected Topics in Signal Processing*, vol. 1, no. 1, pp. 105–113, 2007.

[16] Y. Wei, H. Meng, Y. Liu, and X. Wang, "Radar waveform design for extended target recognition under detection constraints," *Mathematical Problems in Engineering*, vol. 2012, 02 2012.

[17] B. Jiu, H. Liu, D. Feng, and Z. Liu, "Minimax robust transmission waveform and receiving filter design for extended target detection with imprecise prior knowledge," *Signal Processing*, vol. 92, no. 1, pp. 210–218, 2012.

[18] B. Tang and J. Tang, "Robust waveform design of wideband cognitive radar for extended target detection," in *IEEE International Conference on Acoustics, Speech, and Signal Processing*, 2016, pp. 3096–3100.

[19] X. Chen, Q. Yang, B. Deng, and H. Wang, "Robust interference waveform design in fuzzy colored noise based on mutual information," *Journal of Applied Remote Sensing*, vol. 14, p. 1, 03 2020.

[20] X. Du, A. Aubry, A. De Maio, and G. Cui, "Hidden convexity in robust waveform and receive filter bank optimization under range unambiguous clutter," *IEEE Signal Processing Letters*, vol. 27, pp. 885–889, 2020.

[21] H. L. V. Trees, *Detection, Estimation, and Modulation Theory: Radar-Sonar Signal Processing and Gaussian Signals in Noise*. Hoboken, NJ, USA: Wiley, 1971.

[22] C.-Y. Chen and P. P. Vaidyanathan, "MIMO radar waveform optimization with prior information of the extended target and clutter," *IEEE Transactions on Signal Processing*, vol. 57, no. 9, pp. 3533–3544, 2009.

[23] J. Hu *et al.*, "Constant modulus waveform design for MIMO radar via manifold optimization," *Signal Process.*, vol. 190, p. 108322, 2022.

[24] J. Li, G. Liao, Y. Huang, and A. Nehorai, "Manifold optimization for joint design of MIMO-STAP radars," *IEEE Signal Processing Letters*, vol. 27, pp. 1969–1973, 2020.

[25] S. M. Karbasi, A. Aubry, A. De Maio, and M. H. Bastani, "Robust transmit code and receive filter design for extended targets in clutter," *IEEE Transactions on Signal Processing*, vol. 63, no. 8, pp. 1965–1976, 2015.

[26] Z. Xu, J. Zhu, Z. Xie, C. Fan, and X. Huang, "MIMO radar robust waveform-filter design for extended targets based on Lagrangian duality," *IEEE Transactions on Aerospace and Electronic Systems*, vol. 59, no. 2, pp. 1021–1036, 2023.

[27] M. A. Richards, *Fundamentals of Radar Signal Processing*. New York, NY, USA: McGraw-Hill, 2005.

[28] Q. Li, E. Rothwell, K.-M. Chen, and D. Nyquist, "Scattering center analysis of radar targets using fitting scheme and genetic algorithm," *IEEE Transactions on Antennas and Propagation*, vol. 44, no. 2, pp. 198–207, 1996.

[29] Z.-J. Wu, C.-X. Wang, Y.-C. Li, and Z.-Q. Zhou, "Extended target estimation and recognition based on multimodel approach and waveform diversity for cognitive radar," *IEEE Transactions on Geoscience and Remote Sensing*, vol. 60, pp. 1–14, 2022.

[30] S. Haykin, "Cognitive radar: A way of the future," *IEEE Signal Processing Magazine*, vol. 23, no. 1, pp. 30–40, 2006.

[31] B. Tang, J. Liu, H. Wang, and Y. Hu, "Constrained radar waveform design for range profiling," *IEEE Transactions on Signal Processing*, vol. 69, pp. 1924–1937, 2021.

[32] F. Dai, H. Liu, P. Wang, and S. Xia, "Adaptive waveform design for range-spread target tracking," *Electronics Letters*, vol. 46,

pp. 793 – 794, 06 2010.

[33] M. Soltanalian, B. Tang, J. Li, and P. Stoica, "Joint design of the receive filter and transmit sequence for active sensing," *IEEE Signal Processing Letters*, vol. 20, no. 5, pp. 423–426, 2013.

[34] H. Zhang and Z. Zhao, "Joint design of transmit waveforms and receive filters for MIMO radar via manifold optimization," *arXiv preprint arXiv:2102.05457*, 2021.

[35] H. Hayvaci, A. Maio, and D. Erricolo, "Improved detection probability of a radar target in the presence of multipath with prior knowledge of the environment," *IET Radar, Sonar and Navigation*, vol. 7, pp. 36–46, 01 2013.

[36] A. Aubry, A. Maio, M. Piezzo, A. Farina, and M. Wicks, "Cognitive design of the receive filter and transmitted phase code in reverberating environment," *Radar, Sonar & Navigation, IET*, vol. 6, pp. 822–833, 12 2012.

[37] A. Aubry, A. DeMaio, A. Farina, and M. Wicks, "Knowledge-aided (potentially cognitive) transmit signal and receive filter design in signal-dependent clutter," *IEEE Transactions on Aerospace and Electronic Systems*, vol. 49, no. 1, pp. 93–117, 2013.

[38] Y. Yao, A. Farina, and Y. Li, "Robust transmit-receive optimization design for extended target detection," in *2020 IEEE 7th International Workshop on Metrology for AeroSpace (MetroAeroSpace)*, 2020, pp. 22–27.

[39] M. Nouiehed, M. Sanjabi, T. Huang, J. Lee, and M. Razaviyayn, "Solving a class of non-convex min-max games using iterative first order methods," in *Neural Information Processing Systems*, 2019.

[40] M. Razaviyayn, T. Huang, S. Lu, M. Nouiehed, M. Sanjabi, and M. Hong, "Nonconvex min-max optimization: Applications, challenges, and recent theoretical advances," *IEEE Signal Processing Magazine*, vol. 37, no. 5, pp. 55–66, 2020.

[41] C. Jin, P. Netrapalli, and M. Jordan, "What is local optimality in nonconvex-nonconcave minimax optimization?" in *Proceedings of the 37th International Conference on Machine Learning*, ser. Proceedings of Machine Learning Research, H. D. III and A. Singh, Eds., vol. 119. PMLR, 13–18 Jul 2020, pp. 4880–4889.

[42] M. I. Skolnik, *Radar Handbook*. New York, NY, USA: McGraw-Hill, 1990.

[43] L. K. Patton and B. D. Rigling, "Autocorrelation and modulus constraints in radar waveform optimization," in *Proceedings of the IEEE International Waveform Diversity and Design Conference*, 2009, pp. 150–154.

[44] Z.-q. Luo, W.-k. Ma, A. M.-c. So, Y. Ye, and S. Zhang, "Semidefinite relaxation of quadratic optimization problems," *IEEE Signal Processing Magazine*, vol. 27, no. 3, pp. 20–34, 2010.

[45] A. De Maio, Y. Huang, M. Piezzo, S. Zhang, and A. Farina, "Design of optimized radar codes with a peak to average power ratio constraint," *IEEE Transactions on Signal Processing*, vol. 59, no. 6, pp. 2683–2697, 2011.

[46] S. Boyd, N. Parikh, E. Chu, B. Peleato, J. Eckstein *et al.*, "Distributed optimization and statistical learning via the alternating direction method of multipliers," *Foundations and Trends® in Machine learning*, vol. 3, no. 1, pp. 1–122, 2011.

[47] S. Quegan, "Spotlight synthetic aperture radar: Signal processing algorithms." *Journal of Atmospheric and Solar-Terrestrial Physics*, vol. 59, pp. 597–598, 1997.

[48] J. B. Keller, "Geometrical theory of diffraction," *Josa*, vol. 52, no. 2, pp. 116–130, 1962.

[49] C. Bachman, "Some recent developments in RCS measurement techniques," *Proceedings of the IEEE*, vol. 53, no. 8, pp. 962–972, 1965.

[50] W. Dinkelbach, "On nonlinear fractional programming," *Manage. Sci.*, vol. 133, no. 7, pp. 492–498, Mar 1967.

[51] S. Schaible, "Fractional programming. II, on Dinkelbach's algorithm," *Management science*, vol. 22, no. 8, pp. 868–873, 1976.

[52] B. Tang, J. Tuck, and P. Stoica, "Polyphase waveform design for MIMO radar space time adaptive processing," *IEEE Transactions on Signal Processing*, vol. 68, pp. 2143–2154, 2020.

[53] S. Chen, M. He, L. Ran, H. Li, F. Xi, S. Tian, and Z. Liu, "Transmit beampattern synthesis for active RIS-aided MIMO radar

via waveform and beamforming optimization," *IEEE Transactions on Aerospace and Electronic Systems*, pp. 1–13, 2024.

[54] J. Bai, M. Zhang, and H. Zhang, "An inexact ADMM for separable nonconvex and nonsmooth optimization," *Computational Optimization and Applications*, pp. 1–35, 2025.

[55] K. Guo, D. Han, D. Z. Wang, and T. Wu, "Convergence of ADMM for multi-block nonconvex separable optimization models," *Frontiers of Mathematics in China*, vol. 12, pp. 1139–1162, 2017.

[56] J. Bai, J. Li, F. Xu, and H. Zhang, "Generalized symmetric ADMM for separable convex optimization," *Computational optimization and applications*, vol. 70, no. 1, pp. 129–170, 2018.

[57] C. Zhang, Y. Song, X. Cai, and D. Han, "An extended proximal ADMM algorithm for three-block nonconvex optimization problems," *Journal of Computational and Applied Mathematics*, vol. 398, p. 113681, 2021.

[58] Z. Liu, "Nonconvex ADMM for rank-constrained matrix sensing problem," *arXiv preprint arXiv:2310.00660*, vol. v2, 2023.

[59] Y. Wang, W. Yin, and J. Zeng, "Global convergence of ADMM in nonconvex nonsmooth optimization," *Journal of Scientific Computing*, vol. 78, pp. 29–63, 2019.

[60] M. Grant and S. Boyd, "CVX: MATLAB software for disciplined convex programming, version 2.1," Mar. 2014.

[61] S. Diamond and S. Boyd, "CVXPY: A Python-embedded modeling language for convex optimization," *Journal of Machine Learning Research*, vol. 17, no. 83, pp. 1–5, 2016.

[62] A. Agrawal, R. Verschueren, S. Diamond, and S. Boyd, "A rewriting system for convex optimization problems," *Journal of Control and Decision*, vol. 5, no. 1, pp. 42–60, 2018.

[63] S. Sun and A. P. Petropulu, "Waveform design for MIMO radars with matrix completion," *IEEE Journal of Selected Topics in Signal Processing*, vol. 9, no. 8, pp. 1400–1414, 2015.

[64] X. Liu, T. Ballal, M. Ahmed, and T. Y. Al-Naffouri, "Instantaneous GNSS ambiguity resolution and attitude determination via Riemannian manifold optimization," *IEEE Transactions on Aerospace and Electronic Systems*, vol. 59, no. 3, pp. 3296–3312, 2023.

[65] B. Polyak, "The conjugate gradient method in extremal problems," *USSR Computational Mathematics and Mathematical Physics*, vol. 9, no. 4, pp. 94–112, 1969.

[66] J. Li, G. Liao, Y. Huang, Z. Zhang, and A. Nehorai, "Riemannian geometric optimization methods for joint design of transmit sequence and receive filter on MIMO radar," *IEEE Transactions on Signal Processing*, vol. 68, pp. 5602–5616, 2020.

[67] S. Gorshkov, S. Leshchenko, V. Orlenko, and S. Sedyshev, *Radar Target Backscattering Simulation: Software and User's Manual*, ser. Radar Library. Artech House, 2002.

[68] J. D. Shirman, *Computer Simulation of Aerial Target Radar Scattering, Recognition, Detection, Tracking.* Norwood, MA, USA: Artech House, 2002.